Pergamon

Int. J. Heat Mass Transfer. Vol. 39, No. 18, pp. 3781–3790, 1996
Copyright © 1996 Elsevier Science Ltd
Printed in Great Britain. All rights reserved
0017–9310/96 $15.00 + 0.00

PII: S0017-9310(96)00063-4

Condensation on a spray of water drops: a cell model study—I. Flow description

SRINIVAS S. SRIPADA, P. S. AYYASWAMY† and L. J. HUANG

Department of Mechanical Engineering and Applied Mechanics, University of Pennsylvania, Philadelphia, PA 19104-6315, U.S.A.

(*Received* 20 *November* 1995 *and in final form* 8 *February* 1996)

Abstract—A unit cylinder cell model with a body-fitted coordinate system is employed to analyze the hydrodynamics and heat transfer associated with steam condensation on a spray of equal sized water droplets. The droplets are assumed to be moving in the intermediate Reynolds number regime, $Re_g = O(100)$. The distance between neighboring droplet centers is allowed to be arbitrary in the plane of motion, but the droplets are assumed to be uniformly spaced in the plane perpendicular to the direction of motion. Furthermore, once a particular configuration of the droplets is set, the subsequent spacings between the droplet centers in that configuration are taken to remain constant during the entire condensation process. The formulation entails a simultaneous numerical solution of the quasi-steady elliptic partial differential equations that describe the flow field in both the dispersed and continuous phases in each cell. In part I of this study, the results for the velocity, surface pressure and drag are presented. In part II of this study, the results for the condensation induced velocities, surface shear stress, the Nusselt number and the Sherwood number are provided. In both parts of the study, the interactions between neighboring drops have been examined. Copyright © 1996 Elsevier Science Ltd.

1. INTRODUCTION

Most analytical/numerical studies of condensation in published literature have dealt with an isolated droplet (see Ayyaswamy [1, 2]). At present, there is no systematic, careful, and rigorous analysis to report on condensation on a spray of drops. Earlier experimental studies and numerical models, mostly related to nuclear reactor emergency core cooling spray systems, have been discussed in Ayyaswamy [3]. The numerical models have invoked *ad hoc* and questionable assumptions. A brief review of recent experimental research on spray condensation and comparisons of results with the present investigation are provided in part II [4] of this study.

In regard to analyses, many different schemes have been proposed for analyzing phenomena associated with an assemblage of particles (solid particles, drops or bubbles) at various Reynolds numbers. See, for example, Happel [5], Kuwabara [6], Leva [7], Zenz and Othmer [8], Orr [9], Happel and Brenner [10], and LeClair and Hamielec [11]. Most of these studies deal with isothermal, nonphase change situations. Among the many different schemes, the unit-cell approach is commonly employed. In the unit-cell model the assemblage is divided into a number of cells with a single particle occupying each cell. The total problem of a spectrum of particles is then reduced to equivalently solving for the behavior of each single particle in the fluid envelope surrounding it in its cell. The cell shapes are chosen on the basis of geometrical/topological convenience. A cylindrical cell model for describing the hydrodynamics of particle assemblages at intermediate Reynolds numbers has been proposed by Tal and Sirignano [12]; and a multisphere cylindrical cell model for studying the hydrodynamics and heat transfer in an assemblage of evaporating spheres was proposed by Tal *et al.* [13]. These models are also suitable for studying convective situations with condensation. In these models, the Navier–Stokes and energy equations are numerically solved, and the wake effects are taken into account. It is noted that in dealing with a spectrum of moving drops using the cylindrical cell model, sophisticated grid-generation techniques are needed to obtain accurate results, since the drop surface and the bounding surface of the cylindrical cell are dissimilar in geometry. In the vicinity of the drop surface and the cell boundary, the grid points need to conform to the shapes of these surfaces. Many grid generation techniques are available for solving such problems with complex geometries. See, for example, Dwyer and Sanders [14], Dwyer *et al.* [15–18] and Sadhal *et al.* [19]. Among the many numerical techniques available, the differential equation technique appears to be suitable for the condensation study. Dwyer *et al.* [18] have described an adaptive grid method which they have successfully employed for the study of droplet evaporation and combustion. The procedure for establishing transformation metrics between the physical and the computational domains was dis-

† Author to whom correspondence should be addressed.

NOMENCLATURE

c_p specific heat at constant pressure
C drag coefficient
C_D total drag coefficient
d droplet diameter
D_{12} mass diffusivity
e unit vector
Eo Eötvös number ($=g\Delta\rho d^2/\sigma$)
Fo Fourier number ($=\alpha t/R^2$)
g acceleration due to gravity
h heat transfer coefficient
$h1$ cell axial forward half-length
$h2$ cell axial rearward half-length
i unit vector
Ja Jakob number ($=c_{pg}T_\infty/\lambda$)
k thermal conductivity
Le Lewis number ($=\alpha/D$)
m mass fraction
m_1 noncondensable mass fraction
p pressure
Pe Peclet number ($=Ud/\alpha$ or Ud/D)
Pr Prandtl number ($=\nu/\alpha$)
q heat flux
r spherical radial coordinate
$\hat{r}$ cylindrical radial coordinate
R radius of the drop
R_∞ radius of the outer boundary
Re Reynolds number ($=U_\infty d/\nu$)
t time
T temperature
u velocity component
U_∞ free stream velocity
w_1 dimensionless mass fraction ($=m_1/m_{1,\infty}$)
$w1$ cell radius nondimensionalized by drop radius
W condensation parameter ($=1-m_{1,\infty}/m_{1,s}$)
We Weber number ($U^2\rho d/\sigma$)
z cylindrical axial coordinate.

Greek symbols
α thermal diffusivity
$\Delta\rho$ density difference
ζ vorticity
θ spherical polar angle
λ latent heat
μ dynamic viscosity
ν kinematic viscosity
ρ density
σ surface tension
τ stress tensor
ψ stream function.

Subscripts
a arithmetic mean
c condensation
C condensation
F friction
g gaseous phase
l liquid phase
L lead drop
m mean
M mass transfer
P pressure
r radial direction
s at the droplet surface
vs volume-surface (Sauter) mean
θ at angular position
0 at initial time, stagnation value
1 noncondensable
∞ far-stream.

Superscripts
$\bar{}$ average
* dimensionless.

cussed in the study. We employ a similar procedure here.

The present study addresses the fluid mechanics and transport problems associated with condensation in a fundamental manner within the limitations of a cell model (see Happel and Brenner [10]). It may be noted that in a typical spray condensation process of engineering interest, the mass addition to a given droplet during the entire process of condensation is rather small compared to the mass of the droplet. In view of this, cell models may be expected to provide meaningful results for condensation processes, while evaporation or combustion processes which are usually accompanied by significant material depletion may not be described as accurately by such cell models. The interaction between neighboring drops, drag phenomena, and their effects on heat and mass transfer, flow details such as liquid circulation and flow separation have all been discussed in parts I and II [4] of the present study. However, for the sake of brevity, only a selected set of results which bring into focus many novel features associated with multiple particle assemblages have been included here.

2. PHYSICAL DESCRIPTION

Consider a spray of isothermal, cold, equal sized, spherical water drops that is injected into a large volume of saturated steam (condensable) and air (noncondensable). Since the initial temperature of the drops is lower than that of the saturated mixture, condensation of steam occurs on the drop surfaces.

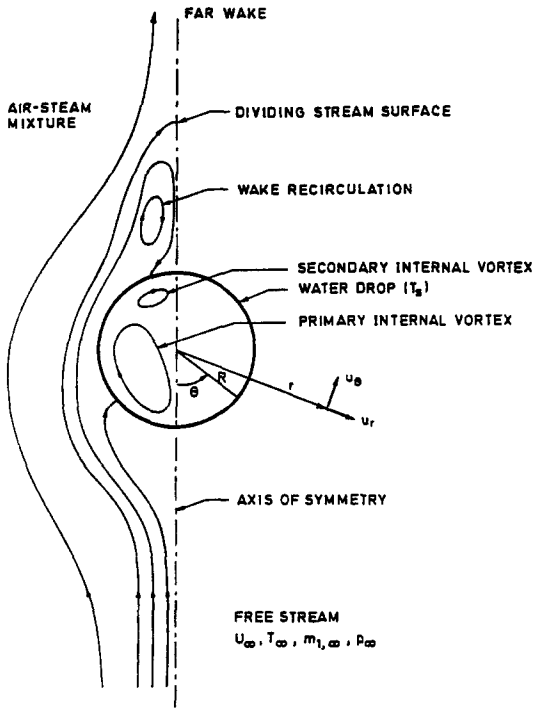

Fig. 1. Flow regions outside and within a droplet at high Reynolds number.

This condensation that is associated with an inward radial flow field offers an important mechanism for heat and mass transfer. Simultaneously, due to droplet translation, the shear stress at the interface initiates liquid circulation inside the drop, as shown in Fig. 1. There is convective heat transfer to the drop interior due to this internal circulation apart from the conductive transport. The noncondensable in the environment accumulates near the drop surface and reduces the rate of condensation by offering diffusional resistance. Detailed discussions of these various effects as related to an isolated droplet are available in the review articles by Ayyaswamy [1, 2].

In this study, we consider an assemblage consisting of a number of cylindrical cells (Fig. 2). Each cell is finite in extent with a radius $w1$ and height $(h1+h2)$, and contains a water drop surrounded by a fluid envelope (Fig. 3). The cell radial ($\hat{r}$) and axial (z) lengths are scaled by the droplet radius R. The fluid envelope is taken to consist of the condensable vapour (steam) and a noncondensable gas (air). Also, each cell is assumed to have the same void ratio as the entire assemblage. The void ratio is defined as the ratio of the volume unoccupied by the drop to the volume of the total cell. The flow around the drop in any individual cell is taken to be axisymmetric. Although, in general, the drop-spray problem may be non-axisymmetric, invoking axisymmetry can indeed serve as a very useful approximation for a reasonably symmetric distribution of neighbors around the flow axis. The distance between neighboring droplet centers is allowed to be arbitrary in the plane of motion, but the droplets are uniformly spaced in the plane perpendicular to the direction of the motion (see Fig. 2). Furthermore, once a particular configuration of the droplets is set, the subsequent spacings between the droplet centers in that configuration are taken to remain constant during the entire condensation process.

The fluid envelope around the drop inside the individual cell is taken to move with an instantaneous bulk velocity U_∞ equal to the instantaneous velocity of the falling drop, i.e. in a coordinate frame fixed to the drop center, the drop would be regarded as stationary with flow around it (Fig. 1). For a gaseous mixture particle in the continuous phase, the typical residence time adjacent to the drop surface is of order R/U_∞. On the other hand, for a liquid particle in the

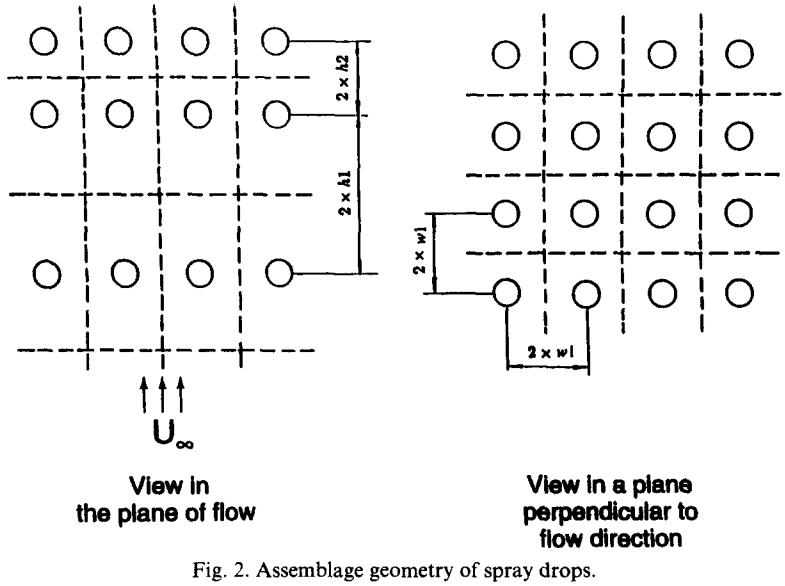

Fig. 2. Assemblage geometry of spray drops.

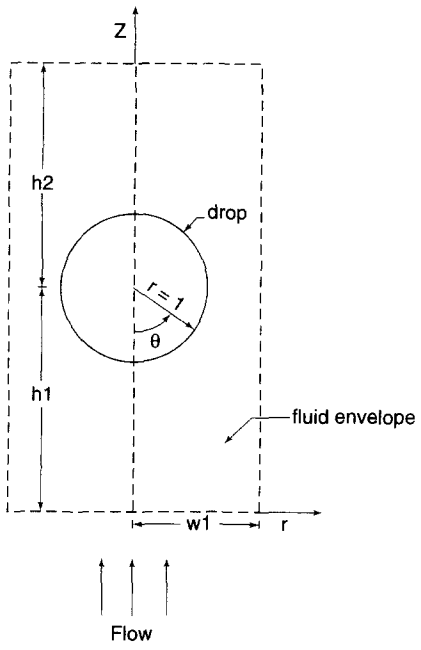

Fig. 3. Geometry and coordinate system of the cylindrical cell model.

dispersed phase, the typical residence time is of order R/U_s, where U_s is the maximum circulation velocity at the drop surface. Since, rapid transients arise due to the sudden contact between the two phases, these residence time estimates are the characteristic times for the rapid transient processes (see Sundararajan and Ayyaswamy [20]). For a circulating water drop translating in a steam–air mixture it is known that (see Law *et al.* [21])

$$\frac{U_s}{U_\infty} = O\left[\left(\frac{\rho_g \mu_g}{\rho_l \mu_l}\right)^{1/3}\right]. \tag{1}$$

Therefore, we have $U_s/U_\infty \approx 10^{-1}$ or less. It may be inferred that the period during which rapid transients occur is of order R/U_s and corresponds to a few circulation cycles inside the drop. Subsequent to this initial period of rapid transients, changes in flow take place at a much slower rate and may be regarded as quasi-steady (see Sundararajan and Ayyaswamy [20] and Huang and Ayyaswamy [22]).

In this study, the Reynolds number of translation (hereinafter referred to as Re_g) is taken to be $O(100)$, but less than, say, 500. For $Re_g > 500$ flow instabilities such as drop oscillations and vortex shedding are known to occur and the flow may not be laminar and the deformation from the spherical shape of the drop may be large (see Sadhal *et al.* [19]). The drop deformation both due to inertial effects (quantified by Weber number We) and due to hydrostatic pressure variation (Eötvös number Eo) will be assumed to be small. We consider water drops of size 1 mm diameter or less ($Eo < 0.4$ and $We < 0.3$). Next, consider the circulation inside the drop. From a shear stress balance across the liquid–gas interface (see Law *et al.* [21]), it may be estimated that $U_s/U_\infty \sim (\rho_g \mu_g/\rho_l \mu_l)^{1/3}$ for $Re_g = O(100)$. Also, $Re_l/Re_g \sim (\rho_l \mu_g^2/\rho_g \mu_l^2)^{2/3}$, where Re_g is the circulation Reynolds number based on U_s. For the range of Re_g considered in the present study, Re_l is also $O(100)$. Condensation causes a radially inward flow towards the drops surface. The nonzero mass flux at the interface alters the translational flow field and modifies the drag on the drop. For $Re_g \sim 100$, flow separates on the rear of the drop. A recirculatory wake is formed whose dimensions in the absence of condensation may be comparable to the drop size (see Clift *et al.* [23]). The radial flow in the presence of condensation drastically reduces the wake size (see Sundararajan and Ayyaswamy [20]), and this feature supports the use of a cell model analysis and lends credibility to the various assumptions made in conjunction with a cell model. The radial flow leads to a build-up of the noncondensable concentration near the drop surface above the level of non-condensable concentration near the cell boundary ('far stream'). The noncondensable accumulation at the droplet surface results in a mass transfer resistance and a consequent reduction in the transport rates. In this study, the effects of noncondensable accumulation, liquid circulation and external-flow separation are taken into account.

3. FORMULATION OF THE MODEL

Apart from the quasi-steady approximation for the hydrodynamics in both phases, some additional assumptions are made in the analysis. These are as follows. (1) Surface tension is large and constant on the interface. (2) Both the liquid and the vapour–gas mixture are pure systems. Surfactants that alter interfacial tension or inhibit condensation by offering interfacial resistance are absent (see Huang and Ayyaswamy [24]). (3) The liquid–vapour interface is in thermodynamic equilibrium; and, nonequilibrium effects due to condensation are negligible. The partial pressure of the vapour at the interface is equal to the vapour pressure corresponding to the drop-surface temperature. The gas–vapour mixture behaves like an ideal gas mixture. The finite condensation rate does not alter the vapour pressure. (4) Property variations with temperature and noncondensable concentration are not included; these variations are not significant in the parameter ranges considered. (5) Viscous dissipation and other compressibility effects are ignored. (6) Radiative heat transfer has been neglected, although gas-phase convective heat transport has been retained for completeness.

The governing equations and boundary conditions for the flow and transport within and outside the drop in a typical cell are now presented.

The nondimensional equations are given by

$$\nabla \cdot \mathbf{u}_g = 0 \tag{2}$$

$$Re_g \mathbf{u}_g \cdot \nabla \mathbf{u}_g = -\tfrac{1}{2} Re_g \nabla p_g + 2\nabla^2 \mathbf{u}_g \quad (3)$$

$$\frac{\partial T_g}{\partial t} + \frac{1}{2} Pe_{g,t} \mathbf{u}_g \cdot \nabla T_g = \nabla^2 T_g \quad (4)$$

$$\frac{\partial w_1}{\partial t} + \frac{1}{2} Pe_{g,m} \mathbf{u}_g \cdot \nabla w_1 = \nabla^2 w_1 \quad (5)$$

$$\nabla \cdot \mathbf{u}_l = 0 \quad (6)$$

$$Re_l \mathbf{u}_l \cdot \nabla \mathbf{u}_l = -\tfrac{1}{2} Re_l \nabla p_l + 2\nabla^2 \mathbf{u}_l \quad (7)$$

$$\frac{\partial T_l}{\partial t} + \frac{1}{2} Pe_l \mathbf{u}_l \cdot \nabla T_l = \nabla^2 T_l. \quad (8)$$

In the above, the subscript g refers to gaseous mixture, 1 to the noncondensable and 2 to the vapour. The asterisks have been omitted for convenience. The velocities $\mathbf{u}_g$ and $\mathbf{u}_l$ have been scaled by U_∞ and the radial coordinate r has been scaled by R. The pressures, Reynolds numbers, temperatures T_g and T_l, mass fraction w_1, Prandtl number Pr_g and Peclet numbers are defined as

$$p_g^* = \frac{p_g - p_\infty}{\frac{1}{2}\rho_g U_\infty^2} \quad p_l^* = \frac{p_l - p_\infty}{\frac{1}{2}\rho_l U_\infty^2}$$

$$Re_g = \frac{U_\infty 2R}{\nu_g} \quad Re_l = \frac{U_\infty 2R}{\nu_l} \quad (9)$$

$$T_g^* = \frac{T_g}{T_\infty} \quad T_l^* = \frac{T_l - T_\infty}{T_0 - T_\infty} \quad w_l^* = \frac{m_1}{m_{1,\infty}} \quad Pr_g = \frac{\nu_g}{\alpha_g} \quad (10)$$

$$Pe_{g,t} = \frac{U_\infty 2R}{\alpha_g} \quad Pe_{g,m} = \frac{U_\infty 2R}{D_{12}} \quad Pe_l = \frac{U_\infty 2R}{\alpha_l}. \quad (11)$$

In equations (4), (5) and (8), time t is scaled by R^2/α_g, R^2/D_{12} and R^2/α_l, respectively. The initial conditions are as follows:

$$T_g = w_1 = 1 \quad \text{for } r > 1 \quad T_l = 1 \quad \text{at } t = 0. \quad (12)$$

The boundary conditions governing the condensation problem are given below.

At the interface (r = 1)

Continuity of tangential velocity

$$u_{g,\theta} = u_{l,\theta}. \quad (13)$$

Continuity of shear stress

$$\mu_g \left[\frac{\partial}{\partial r}\left(\frac{u_{g,\theta}}{r}\right) + \frac{\partial u_{g,r}}{\partial \theta} \right]_{r=1} = \mu_l \left[\frac{\partial}{\partial r}\left(\frac{u_{l,\theta}}{r}\right) + \frac{\partial u_{l,r}}{\partial \theta} \right]_{r=1}. \quad (14)$$

Continuity of mass flux

$$\rho_g (u_{g,r} - \dot{R}) = \rho_l (u_{l,r} - \dot{R}), \quad (15)$$

where $\dot{R}$ is the growth rate of the drop.

Impermeability of the noncondensable

$$\frac{2(1-W)}{Pe_{g,m}} \frac{\partial w_1}{\partial r} = \frac{u_c}{Pe_{g,m}} = u_{g,r}|_{r=1}, \quad (16)$$

where u_c is the nondimensional condensation velocity and is given by $u_c = u_{g,r}|_{r=1} Pe_{g,m}$. The parameter W, referred to as the condensation parameter, is given by $W = 1 - m_{1,\infty}/m_{1,s}$, and it is a function of the thermodynamic conditions p_∞, T_∞ and T_s. W varies from 0 to 1. The limit zero corresponds to a noncondensing situation and $W = 1$ to a pure vapour environment.

Temperature continuity (dimensional)

$$T_g = T_l. \quad (17)$$

Heat flux continuity

$$-Ja_g \frac{\partial T_g}{\partial r} + \frac{1}{2Le_g}\left(u_c + \frac{\rho_g \bar{u}_c}{\rho_l - \rho_g}\right) = q_s, \quad (18)$$

where the Jakob number Ja_g, Lewis number Le_g and nondimensional heat flux q_s^* are given by

$$Ja_g = \frac{c_{pg} T_\infty}{\lambda} \quad Le_g = \frac{\alpha_g}{D_{12}} \quad q_s^* = \frac{q_s R}{\rho_g \alpha_g \lambda} \quad (19)$$

and c_{pg} is specific heat, λ is the latent heat of condensation. In the above, the dimensional heat flux q_s into the liquid phase is given by

$$q_s = -k_l \left.\frac{\partial T_l}{\partial r}\right|_{r=1}. \quad (20)$$

The quantity $\bar{u}_c^*$ is the average value of the u_c over the surface and is given by

$$\bar{u}_c = \frac{1}{2}\int_0^\pi u_c \sin\theta \, d\theta. \quad (21)$$

Normalized mass fraction at interface

$$w_1 = w_s, \quad (22)$$

where w_s can be evaluated by using the Clapeyron equation with the assumption of local thermodynamic equilibrium.

At the inlet of the cell containing the lead drop(s)

Uniform velocity

$$\mathbf{u}_g = \mathbf{i}_z \quad (23)$$

where $\mathbf{i}_z$ is the unit vector along the axis of symmetry.

Bulk mixture conditions

$$T_g = 1 = w_1 \quad p_g = 0. \quad (24)$$

At the inlet of the cell containing the follower drop(s)

Continuity of velocity

$$u_{g,r} = 0 \quad (25)$$

$$u_{g,z}|_{\text{inlet}} = u_{g,z}|_{\text{exit of the cell ahead}}. \quad (26)$$

Continuity of temperature and species

$$T_g|_{\text{inlet}} = T_g|_{\text{exist of the cell ahead}} \quad (27)$$

$$w_l|_{\text{inlet}} = w_l|_{\text{exit of the cell ahead}}. \quad (28)$$

At the exit of each cell

$$u_{g,\hat{r}} = \frac{\partial u_{g,z}}{\partial z} = 0 \quad (29)$$

$$\frac{\partial T_g}{\partial z} = 0 \quad (30)$$

$$\frac{\partial w_l}{\partial z} = 0. \quad (31)$$

On each cell envelope

$$u_{g,\hat{r}} = \frac{\partial u_{g,z}}{\partial \hat{r}} = \frac{\partial p_g}{\partial \hat{r}} = \frac{\partial T_g}{\partial \hat{r}} = \frac{\partial w_l}{\partial \hat{r}} = 0. \quad (32)$$

Axisymmetric conditions at $\theta = 0$ and π in each cell

$$u_{g,\hat{r}} = \frac{\partial u_{g,z}}{\partial \hat{r}} = \frac{\partial p_g}{\partial \hat{r}} = \frac{\partial T_g}{\partial \hat{r}} = \frac{\partial w_l}{\partial \hat{r}} = 0 \quad (33)$$

$$u_{l,\theta} = \frac{\partial u_{l,l}}{\partial \theta} = \frac{\partial p_l}{\partial \theta} = \frac{\partial T_l}{\partial \theta} = 0. \quad (34)$$

4. SOLUTION PROCEDURE

We recall that the unit-cell formulation of condensation on a spray of drops involves the specification of several parameters. These are: (i) the steam–air mixture conditions: pressure p_∞ and temperature T_∞; (ii) the drop initial conditions at the spray-nozzle outlet: initial radius R_0, velocity U_0 and initial temperature T_0; (iii) parameters describing the relative geometry between a typical drop and its neighbors in the spray; these are reflected in the specification of the cell height h_1 and h_2, and radius $w1$ (Fig. 3). The intention is to quantitatively estimate the influence of each of the above mentioned parameters on flow and transport associated with a typical drop enclosed in a unit-cell.

An examination of the unit-cell formulation reveals that the governing equations (2)–(8), along with the initial and boundary conditions, are a set of coupled, nonlinear partial differential equations. The simultaneous solution of these equations requires an iterative computational procedure involving stable numerical schemes. A numerical procedure that is based on the hybrid difference scheme is employed here. This scheme is a combination of a second-order accurate central difference scheme (CDS) and a first-order accurate upwind difference scheme (UDS) (see Sundararajan and Ayyaswamy [25]). The generation of the computational grid requires more detailed considerations. Sophisticated grid-generation techniques are needed to obtain accurate results, since the drop surface and the bounding surface of the cylindrical cell are dissimilar in geometry. In the vicinity of the drop surface and the cell boundary, the grid points need to conform to the shapes of these surfaces. Novel grid-generation techniques have been proposed for solving problems with complex geometries (see Thompson *et al.* [26]). Here, we employ the body-fitted coordinate system for grid generation. The particular form employed in this study was first developed and applied to fluid mechanical problems by Thompson *et al.* [26] and later has been successfully used by Dwyer *et al.* [18].

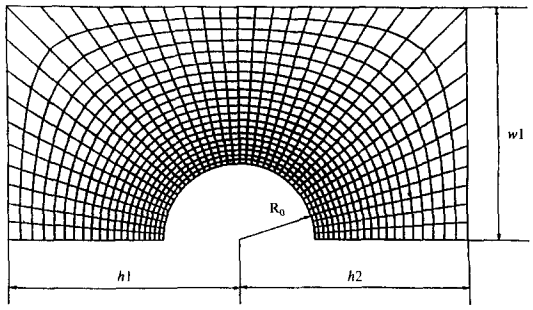

Fig. 4. Body fitted grid system for the cylindrical cell model.

With a body-fitted coordinate system for grid generation (Fig. 4), and a hybrid scheme for finite differencing the equations and boundary conditions, we choose to employ the alternating direction implicit procedure (ADI) for iteration. Since the generated grid is non-orthogonal, the finite difference equations must be suitably modified. Details of such modifications are available in Huang [27]. The governing equations and boundary conditions of the unit-cell model are solved using the dimensionless stream function ψ (scaled with $U_\infty R^2$) and vorticity ζ (scaled with U_∞/R). In spherical coordinates (Fig. 1) the stream function and vorticity are defined by

$$\mathbf{u}_g = \nabla \times \left[-\frac{\psi_g}{r \sin\theta} \mathbf{e}_\phi \right] \quad (35)$$

$$\psi_g \mathbf{e}_\phi = \nabla \times \mathbf{u}_g \quad (36)$$

$$\mathbf{u}_l = \nabla \times \left[-\frac{\psi_l}{r \sin\theta} \mathbf{e}_\phi \right] \quad (37)$$

$$\psi_l \mathbf{e}_\phi = \nabla \times \mathbf{u}_l. \quad (38)$$

The solution domain of the gas phase is divided into a grid of variable size. A fine spacing is employed near the drop, where the gradients are steep. A coarse spacing is adequate in the far stream, where the gradients are weak. As the dependent variables evolve (with time or with iterations), the grid structure also evolves, in the physical domain. Typically, grids with 91×61 exterior nodes and 61×61 interior nodes have been used. The nonlinear algebraic difference equations are solved iteratively, starting from suitable guess solutions. The number of iterations required to attain convergence is significantly reduced by noting that the flow inside the drop may be approximated for the first iteration as a Hill's spherical vortex of reduced strength. On this basis, the values of the velocity components at the beginning of the iterative procedure for the flow and heat transfer are set at:

$$u_r \sim 0.1(1-r^2)\cos\theta \quad u_\theta \sim 0.1(1-2r^2)\sin\theta. \tag{39}$$

The factor 0.1 approximately accounts for the effect of liquid viscosity on the strength of the Hill's spherical vortex solution in the intermediate Reynolds number range of drop motion (see Chung and Ayyaswamy [28]). A successive over relaxation (SOR) procedure is used to accelerate convergence. Computations are carried out until the changes in the predicted transport quantities are less than 10^{-7} (absolute error) or less than 0.1% (relative error) between successive iterations. The time for a typical computer run is of the order of 1 CPU s on the Pittsburgh Supercomputer CRAY X/MP.

5. PHYSICAL QUANTITIES OF THE PROBLEM

In this section, equations are presented for obtaining the pressure profile, stress and drag coefficients. The total drag coefficient C_D is

$$C_D = C_F + C_P + C_C, \tag{40}$$

where the friction drag coefficient C_F is

$$C_F = \frac{8}{Re_g}\int_0^\pi (\tau_{r\theta}\sin\theta - \tau_{rr}\cos\theta)_{r=1}\sin\theta\,d\theta \tag{41}$$

with shear stress

$$\tau_{r\theta} = \left[r\frac{\partial}{\partial r}\left(\frac{u_{g,\theta}}{r}\right) + \frac{1}{r}\frac{\partial u_{g,r}}{\partial\theta}\right]_{r=1} \tag{42}$$

and normal stress

$$\tau_{rr} = 2\frac{\partial u_{g,r}}{\partial r}\bigg|_{r=1}. \tag{43}$$

The pressure drag coefficient C_P is

$$C_P = \int_0^\pi p_{g,s}\sin 2\theta\,d\theta \tag{44}$$

and the condensation drag C_C is

$$C_C = 4\int_0^\pi [(u_{g,r}\cos\theta - u_{g,\theta}\sin\theta)u_{g,r}\sin\theta]_{r=1}\,d\theta. \tag{45}$$

In equation (44), the surface pressure profile $p_{g,s}$ may be obtained from the vorticity equation. For this purpose, consider the vorticity equation

$$\nabla(u_g^2 + p_g) = 2\mathbf{u}_g \times (\zeta_g \mathbf{e}_\phi) - \frac{4}{Re_g}\nabla\times(\zeta_g\mathbf{e}_\phi), \tag{46}$$

where

$$u_g^2 = u_{g,r}^2 + u_{g,\theta}^2. \tag{47}$$

For the lead drop,

$$p_{g,s} = p_{g,0} + [u_{g,r}^2|_{\theta=0} - u_g^2]_{r=1} + \int_0^\theta \left[-2u_{g,r}\zeta_g + \frac{4}{Re_g}\left(\zeta_g + \frac{\partial\zeta_g}{\partial r}\right)\right]_{r=1} d\theta, \tag{48}$$

where the gas phase stagnation pressure $p_{g,0}$ is obtained by an integration of the r-component of equation (46) along $\theta = 0$

$$p_{g,0} = 1 - \left[u_{g,r}^2|_{r=1} - \frac{8}{Re_g}\int_1^{h_1}\frac{1}{r}\frac{\partial\zeta_g}{\partial\theta}dr\right]_{\theta=0}. \tag{49}$$

For the follower drop(s), the gas phase stagnation pressure $p_{g,0}$ is obtained by an integration of the r-component of equation (46) along $\theta = 0$

$$p_{g,0} = p_{g,e} + u_{g,e}^2 - \left[u_{g,r}^2|_{r=1} - \frac{8}{Re_g}\int_1^{h_1}\frac{1}{r}\frac{\partial\zeta_g}{\partial\theta}dr\right]_{\theta=0}, \tag{50}$$

where $u_{g,e}$ is the exit velocity at $\theta = \pi$ of the drop ahead and $p_{g,e}$ is the exit pressure at $\theta = \pi$ of the drop ahead. The exit pressure $p_{g,e}$ is given by

$$p_{g,e} = p_{g,\pi} + \left[u_{g,r}^2|_{r=1} - u_{g,r}^2|_{r=h_2} - \frac{8}{Re_g}\int_1^{h_2}\frac{1}{r}\frac{\partial\zeta_g}{\partial\theta}dr\right]_{\theta=\pi} \tag{51}$$

and $p_{g,\pi}$ is the surface pressure at $\theta = \pi$ of the drop ahead. With $p_{g,0}$ known for the follower drop, the surface pressure profile $p_{g,s}$ may be evaluated from equation (48), which is applicable for any drop.

6. RESULTS AND DISCUSSION

The hydrodynamic results are presented for various values of Re_g and for $W = 0.41$.

In Fig. 5, the dimensionless exit velocities at $\theta = \pi$ (outlets of the cells containing the lead drop A, and the follower drops B, C, D which are traveling in tandem) have been plotted for $W = 0.41$, $Re_g = 20$ and 100, and $h1 : w1 : h2 = 5 : 5 : 5$. The cells will hereinafter be identified by the name of the drop it contains, e.g. cell A, cell B, and so on. For potential

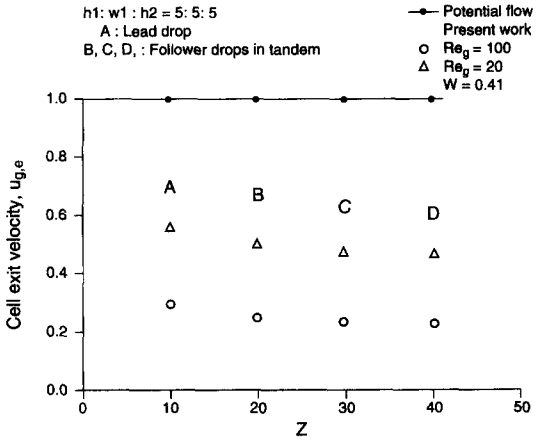

Fig. 5. The cell exit velocity $u_{g,e}$ of drops A, B, C and D.

flow, the nondimensional cell-exit velocity $u_{g,e}$ will equal unity which is the same as the free stream value at the entrance to cell A. For $W = 0.41$ and the range of Re_g shown, the reduction in actual exit velocities compared to the potential flow value are primarily due to viscous effects. We recall that condensation is like suction and the vorticity is convected radially towards the drop surface during condensation. This results in thinner boundary layers and therefore higher viscous shear stresses and friction drag. For a given drop, at a fixed W, the decrease in velocity as the flow traverses the cell is larger at a higher Re_g, irrespective of the position of the drop in the array. This can be explained by noting that at a fixed W, higher values of Re_g result in higher levels of condensation and these in turn lead to higher friction drag forces. We note that there is a significantly larger decrease in the velocity during flow through cell A compared with the decreases experienced in cells B, C and D. This is explained by noting that the lead drop experiences more vigorous condensation and there is a corresponding decrease in the flow velocity at the exit of the lead cell. The reduced flow velocity at the inlet of cell B implies a relatively less vigorous condensation over drop B and therefore, the reduction in flow velocity is less drastic during the traverse over drop B. This effect is even more pronounced with drops C and D.

In Fig. 6, the exit pressure values $p_{g,e}$ at the cell outlets for $Re_g = 100$, $W = 0.41$, and $h1 : w1 : h2 = 5 : 5 : 5$ are compared with those for a potential flow solution. The higher pressure compared to potential flow at the exit of cell A is due to pressure recovery at the rear of drop A, that is associated both with vigorous condensation (see Sundararajan and Ayyaswamy [20]) and a decrease in flow velocity. For high enough W, the large pressure recovery associated with condensation may actually result in a negative pressure drag (see Sundararajan and Ayyaswamy [20]). In cells B, C and D, for the prevailing conditions, the flow velocity is smaller compared to that in cell A, and the condensation is correspondingly at a lower level. As a result, the exit pressure values are lower than those at the inlet due to reduced pressure recovery and these would correspond to positive pressure drag values. However, for different inlet conditions, these features may be different. This is in view of the competing mechanisms of pressure recovery (pressure drag) and reduction of flow velocity (viscous drag). These mechanisms together control the dynamics of the drop.

For drops A, B, C and D, the gaseous phase pressure profile $p_{g,s}$ at the drop surface changes drastically with position, as shown in Fig. 7, which is plotted for the same parameter values as for Fig. 6. For a given drop, the stagnation point pressure has the highest value. From equation (48), it is clear that the pressure profile is predominantly determined from a balance between the diffusive and the convective transports of vorticity. Without condensation, the diffusion of vorticity away from the drop causes pressure loss in the rear. With condensation, the radially inward flow counters this outward diffusion of vorticity. Stagnation point pressures for follower drops are lower in view of the effects of recirculation in the wake regions of leader drops. Also, the pressure recovery at the rear of the follower drops is lower because of the reduced levels of condensation.

The hydrodynamics associated with a row of the drops are also strongly influenced by the presence of drops on the sides. If the side drops are sufficiently distant from any given drop, for example, $w1 > 10$ for $Re_g = 100$, the effects of the side drops are negligible.

The gaseous phase pressure profile at the surface of a typical drop, $p_{g,s}$, is influenced drastically by the presence of the side drops, as shown in Fig. 8 for $W = 0.41$, $Re_g = 100$, and various lateral drop spacings. As the lateral drops come closer to the drop under consideration (drop A), the effective flow velocity around drop A increases due to the constriction of flow volume. As a result, the effective Reynolds number increases, the strength of recirculation in the wake region is higher and the volume of the wake is larger. For the parameters under consideration, the

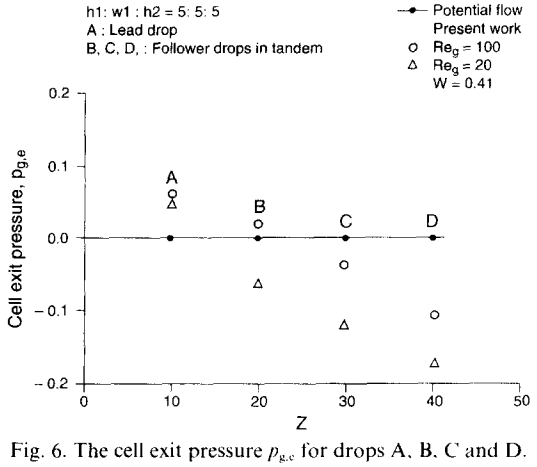

Fig. 6. The cell exit pressure $p_{g,e}$ for drops A, B, C and D.

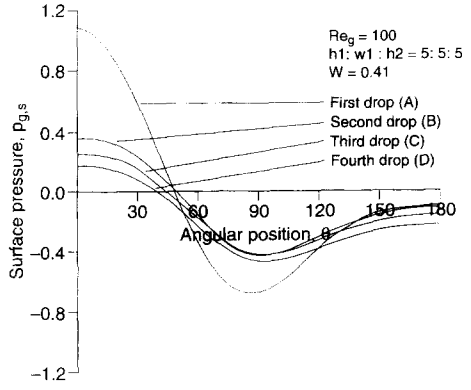

Fig. 7. The variation of surface pressure $p_{g,s}$ with angular location for drops A, B, C and D.

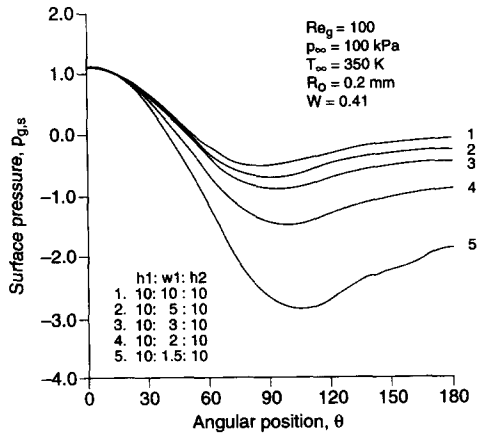

Fig. 8. The variation of surface pressure $p_{g,s}$ for the lead drop with the angular location for various lateral spacings of the side drops.

pressure recovery at the rear of the drop A becomes smaller as the lateral drops get closer. Again, these trends may not be the same for different parameter values of Re_g and W. It may be argued that with an increased effective Re_g, the level of condensation would increase and the wake volume would reduce. But, for the $Re_g = 100$, $W = 0.41$ combination, the effect of increase in the level of condensation due to the increased effective Re_g appears to be more than offset by the reduced pressure recovery associated with higher friction.

The variation in the drag coefficients for lead drop A for various spacings of the lateral drops, $w1$, is shown in Fig. 9. The parameters are $Re_g = 100$ and $W = 0.41$. The coefficients for the friction drag C_F, the condensation drag C_C, and the pressure drag C_P increase with the proximity of the side drops (lower values of $w1$). The C_F increases with proximity of the side drops, due to the increased shear stress that is a consequence of the constriction of the flow. The C_C,

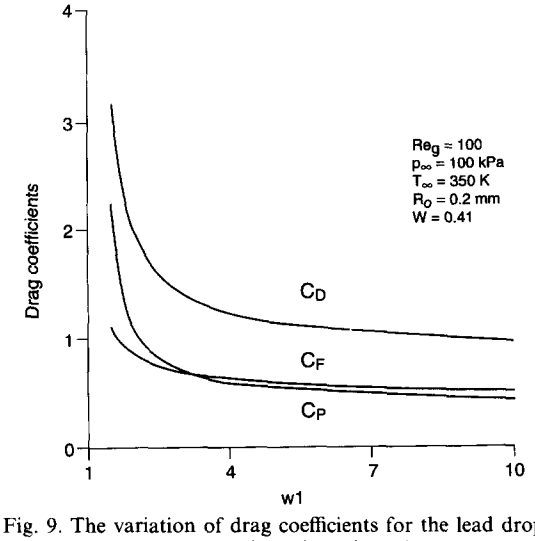

Fig. 9. The variation of drag coefficients for the lead drop with varying lateral spacing $w1$.

which arises owing to the momentum of the radial inflow, increases with proximity of the side drops due to increased convective velocity. The increase in C_P is because of the reduced pressure recovery in the rear of the drop due to the larger wake volume. Again, it should be emphasized that in view of the complex nature of the interactions between the various drag mechanisms in condensing situations, very specific conclusions regarding the influence of drops on the sides cannot be drawn. Rather, some general features may be discerned by studies such as the one presented here.

7. CONCLUSIONS

The hydrodynamics associated with steam condensation on a spray of equal sized water droplets has been analyzed, employing a unit cylinder cell model with a body-fitted coordinate system. The droplets have been assumed to translate in the intermediate Reynolds number regime, $Re_g = O(100)$. There is a reduction in cell exit velocities owing primarily to viscous effects. The condensation-induced radial inflow acts like suction that results in vorticity to be convected towards the drop surface. The cell pressure computations show that there is significant pressure recovery at the rear of the drops, owing both to vigorous condensation and to a decrease in the exit velocity. For high enough condensation rates, the resultant pressure recovery may actually cause the development of a negative pressure drag. The surface pressure profile results indicate that it is predominantly determined by a balance between the diffusive (radially outward) and convective (radially inward) transport of vorticity. The gaseous phase profiles are also drastically influenced by proximity of the side drops. For the parameters considered, the constriction of flow cross-section with a higher proximity of drops, causes an increase in wake volume and consequently reduced pressure recovery.

The formulation and solution procedure presented here is also used to evaluate shear stress, and the heat/mass transport quantities. The results for the transport quantities are presented in part II [4].

Acknowledgements—The numerical calculations were made on the Pittsburgh Supercomputer under NSF grant ECS-0000000/8515068. The authors are grateful for the Pittsburgh Supercomputer Center services and to NSF.

REFERENCES

1. P. S. Ayyaswamy, Direct contact transfer processes with moving liquid droplets. In *Advances in Heat Transfer* (Edited by J. P. Hartnett, T. F. Irvine, Jr and Y. I. Cho). Academic Press, New York (1995).
2. P. S. Ayyaswamy, Mathematical methods in direct-contact transfer studies with droplets. In *Annual Review of Heat Transfer* (Edited by C. L. Tien), Vol. 6. Begell House, New York (1995).
3. P. S. Ayyaswamy, Fluid mechanics of direct-contact transfer processes with moving liquid droplets. In *Encyclopedia of Fluid Mechanics* (Edited by N. P. Cher-

emisinoff), Chap. 16. Gulf Publishing, Houston, TX (1989).
4. L. J. Huang, P. S. Ayyaswamy and S. S. Sripada, Condensation on a spray of water drops : a cell model study—II. Transport quantities, *Int. J. Heat Mass Transfer* **39,** 3751–3757 (1996).
5. J. Happel, Viscous flow in multiparticle system : slow motion of fluids relative to beds of spherical particles, *AIChE J.* **4,** 197–201 (1958).
6. S. Kuwabara, The forces experienced by randomly distributed parallel circular cylinders or spheres in a viscous flow at small Reynolds numbers, *J. Phys. Soc. Jap.* **14,** 527–532 (1959).
7. M. Leva, *Fluidization*. McGraw-Hill, New York (1959).
8. R. A. Zenz and D. F. Othmer, *Fluidization and Fluid Particle Systems*. Reinhold, New York (1960).
9. C. Orr, *Particle Technology*. MacMillan, New York (1966).
10. J. Happel and H. Brenner, *Low Reynolds Number Hydrodynamics*. Noordhoff, Leyden, Holland (1973).
11. B. P. LeClair and A. E. Hamielec, Viscous flow through particle assemblages at intermediate Reynolds numbers, *I & EC Fundam.* **7,** 543–548 (1968).
12. R. Tal and W. A. Sirignano, Cylindrical cell model for the hydrodynamics of particle assemblages at intermediate Reynolds numbers, *AIChE J.* **28,** 233–236 (1982).
13. R. Tal, D. N. Lee and W. A. Sirignano, Hydrodynamics and heat transfer in sphere assemblages—cylindrical cell models, *Int. J. Heat Mass Transfer* **26,** 1265–1273 (1983).
14. H. A. Dwyer and B. R. Sanders, Numerical modeling of unsteady flame propagation, *Acta Astronaut.* **5,** 1171–1184 (1978).
15. H. A. Dwyer, R. J. Kee, P. K. Barr and B. R. Sanders, Transient droplet heating at high Peclet number, *J. Fluids Engng Trans. ASME* **105,** 83–88 (1983).
16. H. A. Dwyer, R. J. Kee and B. R. Sanders, Adaptive grid method for problems in fluid mechanics and heat transfer, *AIAA J.* **18,** 1205–1212 (1980).
17. H. A. Dwyer, H. Nirschl, P. Kerschl and V. Denk, Heat, mass and momentum transfer about arbitrary groups of particles, *Proceedings of the Twenty-fifth Symposium (International) on Combustion*, pp. 389–395. The Combustion Institute, Pittsburgh, PA (1994).
18. H. A. Dwyer, B. R. Sanders and F. Raiszadek, Ignition and flame propagation studies with adaptive numerical grids, *Combust. Flame* **52,** 11–23 (1983).
19. S. S. Sadhal, P. S. Ayyaswamy and J. N. Chung, *Transport Phenomena with Drops and Bubbles*. Springer, Berlin (1996).
20. T. Sundararajan and P. S. Ayyaswamy, Hydrodynamics and heat transfer associated with condensation on a moving drop : solutions for intermediate Reynolds numbers, *J. Fluid Mech.* **149,** 33–58 (1984).
21. C. K. Law, S. Prakash and W. A. Sirignano, Theory of convective, transient, multicomponent droplet vaporization, *Proceedings of the Sixteenth Symposium (International) on Combustion*, pp. 605–617. The Combustion Institute, Pittsburgh, PA (1977).
22. L. J. Huang and P. S. Ayyaswamy, Heat and mass transfer associated with a spray drop experiencing condensation : a fully transient analysis, *Int. J. Heat Mass Transfer* **30,** 881–891 (1987).
23. R. Clift, J. R. Grace and M. E. Weber, *Bubbles, Drops and Particles*. Academic Press, New York (1978).
24. L. J. Huang and P. S. Ayyaswamy, Effect of insoluble surfactants in condensation on a moving drop, *J. Heat Transfer* **113,** 232–236 (1991).
25. T. Sundararajan and P. S. Ayyaswamy, Numerical evaluation of heat and mass transfer to a moving liquid drop experiencing condensation, *Numer. Heat Transfer* **8,** 689–706 (1985).
26. J. F. Thompson, F. C. Thames and C. W. Mastin, Automatic numerical generation of body-fitted curvilinear coordinate system for field containing any number of arbitrary two-dimensional bodies, *J. Comput. Phys.* **15,** 299–319 (1974).
27. L. J. Huang, Fundamental problems in heat transfer and fluid mechanics of phase change processes with liquid drops, Ph.D. thesis, University of Pennsylvania, PA (1989).
28. J. N. Chung and P. S. Ayyaswamy, Laminar condensation heat and mass transfer to a moving drop, *AIChE J.* **27,** 372–377 (1981).